Dynamics of two trapped Brownian particles: shear-induced cross-correlations

Jochen Bammert, Lukas Holzer, Walter Zimmermann

Theoretische Physik I, Universität Bayreuth, D-95440 Bayreuth

(Dated: Received: October 25, 2010/ Revised version: October 25, 2010)

The dynamics of two Brownian particles trapped by two neighboring harmonic potentials in a linear shear flow is investigated. The positional correlation functions in this system are calculated analytically and analyzed as a function of the shear rate and the trap distance. Shear-induced cross-correlations between particle fluctuations along orthogonal directions in the shear plane are found. They are linear in the shear rate, asymmetric in time, and occur for one particle as well as between both particles. Moreover, the shear rate enters as a quadratic correction to the well-known correlations of random displacements along parallel spatial directions. The correlation functions depend on the orientation of the connection vector between the potential minima with respect to the flow direction. As a consequence, the inter-particle cross-correlations between orthogonal fluctuations can have zero, one or two local extrema as a function of time. Possible experiments for detecting these predicted correlations are described.

I. INTRODUCTION

The Brownian dynamics of particles in fluids is of high relevance in many fields of natural and applied sciences. It is strongly affected by the interplay between the particles via the liquid, the so-called hydrodynamic interaction. Especially in the field of microfluidics this nonlinear interaction plays an important role in subjects such as Taylor dispersion [1] or fluid mixing [2, 3]. In a quiescent fluid there is already a considerable understanding of the dynamics of Brownian particles and their interactions [4, 5]. Investigations on the positional correlation functions of two trapped particles give further insight in the coupling between thermal motion and the hydrodynamic interaction among them [6, 7]. However, the understanding of this interplay in typical laminar flows, like in a linear shear flow or in a Poiseuille flow, is still far from complete although it is the origin of a number of interesting phenomena. For example, polymers exhibit in shear flows already at small values of the Reynolds number the so-called molecular individualism [8, 9], elastic turbulence, and spectacular mixing properties in the dilute regime [10]. The complex interplay between Brownian motion and hydrodynamic interaction also affects considerably the conformational distribution functions of tethered polymers in flows and their dynamics [11–19]. When polymers are attached to a wall and subjected to a flow, an additional time-periodic behavior influences the dynamics [20–24], which shows similar features as tumbling polymers in shear flows [8, 25–27].

Recent theoretical investigations on the fluid-velocity fluctuations in shear flows show that in contrast to quiescent fluids or uniform flows, cross-correlations between velocity fluctuations along and perpendicular to the streamlines occur [28, 29]. For free Brownian particles in a linear shear flow in x direction, where the shear plane is parallel to the xy plane, one also expects a cross-correlation between the orthogonal positional fluctuations $\tilde{x}$ and $\tilde{y}$ of the particles, i.e. $\langle \tilde{x}\tilde{y} \rangle \neq 0$ [30–32]. In this case, random jumps of a particle between neighboring parallel streamlines lead to a change of the particle's velocity. For example, a positional fluctuation, $\tilde{y}$, perpendicular to the streamlines may cause a fluctuation, $\tilde{x}$, along the streamlines and contributes in this way to the correlation function $\langle \tilde{x}\tilde{y} \rangle$, which reflects the shear-induced coupling between fluctuations along orthogonal directions.

The theoretical considerations described in Ref. [33] show that shear-induced cross-correlations between perpendicular random particle displacements, like $\langle \tilde{x}\tilde{y} \rangle \neq 0$, survive if a particle experiences some constraints such as a harmonic potential. This is important from various points of view. First, these cross-correlations are inherently present in bead-spring models, which are used to describe polymer dynamics in shear flows, because the individual beads along the chain are bound to their neighbors. Second, this knowledge facilitates the experimental detection of these cross-correlations, because measurements of particle fluctuations in the spatially limited area of the trapping potential can be performed in a controlled manner compared to tracing free Brownian particles. According to this strategy, the cross-correlations $\langle \tilde{x}\tilde{y} \rangle$ of trapped particles in a linear shear flow have been measured directly for the first time and the results are in good agreement with the theoretical predictions [34].

The optical tweezer technique, employed in Ref. [34], triggered a number of further direct observations of particle fluctuations. These include inspiring studies on single polymers [11–13, 35], the propagation of hydrodynamic interactions [36], wall effects on Brownian motion [37, 38], two-point microrheology [39], particle sorting techniques [40–43], the determination of the effective pair potential in colloidal suspensions [44], and many other investigations in microfluidics, cf. [45, 46]. By femto-Newton measurements anti-correlations have been detected between two hydrodynamically interacting and

neighboring particles in a quiescent fluid, each one captured by a laser-tweezer potential [6]. This was recently extended in Ref. [34], where shear-induced inter-particle anti-correlations between orthogonal motions of the two particles have been found.

The present work focuses on the question, which kind of cross-correlations can be expected between hydrodynamically interacting particles in linear shear flows. Such inter-particle correlations along a single polymer and between different polymers in flows influence their dynamics. This paper is an extension of the theoretical work on the single particle dynamics described in Ref. [33] to a pair of two hydrodynamically interacting point-particles with an effective hydrodynamic radius and trapped in a linear shear flow. It provides the theoretical background for the experimental results on the two-particle correlations presented in Ref. [34]. The correlation functions between the different particle displacements are calculated analytically and we show how a second Brownian particle influences the stochastic motion and the positional probability distribution of its neighbor compared to the single particle case [33, 34]. In addition, we find that the anti cross-correlations between two fluctuating particles in a quiescent fluid, as described in Ref. [6], experience shear-induced corrections. We also describe the occurrence of shear-induced anti cross-correlations between the fluctuations of the two particles along two orthogonal directions. The results depend significantly on the orientation of the connection vector between the two traps with respect to the flow direction. We focus on the leading order contributions to the correlation functions and neglect the effects of finite size and rotations of the particles.

The structure of the paper is as follows: In sect. II, the model equations are introduced and their formal analytical solution is presented, which results in the calculation of the correlation functions for the random particle displacements. In sect. III, the results for three representative setups of the two-particle system are discussed in detail, where the connection vector between the two potential minima is either parallel, perpendicular, or oblique to the shear-flow direction. In addition, the results are compared with direct simulations of the Langevin equation for representative examples. For the parallel case, a few experimental and theoretical results have already been described in Ref. [34], where a good agreement between experiment and theory was found. The article closes with a discussion and further possible applications in sect. IV.

II. EQUATIONS OF MOTION AND THEIR SOLUTION

The basis of our investigation is a Langevin model that describes the over-damped dynamics of two particles, each held by a harmonic potential in a linear shear flow. In this section the equation of motion is introduced and solved in order to calculate the correlation functions analytically. They consist of different eigenmodes, which
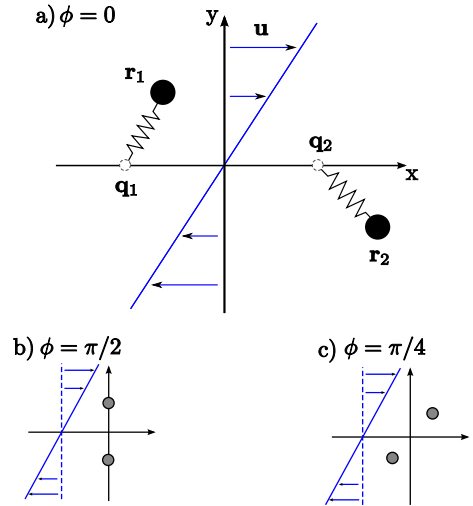

FIG. 1. Two Brownian particles are kept by linear spring-forces $\mathbf{f}_{1,2}^V$ close to the minima of two corresponding harmonic potentials at $\mathbf{q}_{1,2}$. Both particles are simultaneously exposed to a linear shear flow $\mathbf{u}(\mathbf{r})$. The angle ϕ between the flow direction $\mathbf{u}(\mathbf{r})$ and the vector $\mathbf{q}_{12} = \mathbf{q}_1 - \mathbf{q}_2$ connecting the potential minima at the distance $d = |\mathbf{q}_{12}|$ is either zero, as in part a), or $\phi = \pi/2$ as in b), or $\phi = \pi/4$ as in c).

are discussed briefly.

A. Model equations

We consider two Brownian point-particles with effective hydrodynamic radius a, immersed in a Newtonian fluid of viscosity η at the positions $\mathbf{r}_i = (x_i, y_i, z_i)$ with $i = 1, 2$. Each particle is held by a linear restoring force,

$$\mathbf{f}_i^V = -\nabla V_i = -k\left(\mathbf{r}_i - \mathbf{q}_i\right), \qquad (1)$$

close to the minimum $\mathbf{q}_i$ of a corresponding harmonic potential,

$$V_i = \frac{k}{2}\left(\mathbf{r}_i - \mathbf{q}_i\right)^2, \qquad (2)$$

with the spring constant k. The distance between the potential minima is labeled with d. Uncharged polystyrene latex beads of micrometer size that are trapped by laser tweezers experience such a potential as described by eq. (2) [6, 47, 48].

Both trapped particles are exposed to a linear shear flow in the x direction with the shear plane parallel to the xy plane and the shear rate $\dot{\gamma}$:

$$\mathbf{u}(\mathbf{r}) = \dot{\gamma} y \mathbf{e}_x. \qquad (3)$$

This flow causes a drag force on the hydrodynamically interacting Brownian particles, which is in competition with the restoring force (1). In a recent experiment the interplay between these two forces has been studied [34],

where the size of the particles was about $5\mu m$ and the shear rate about $50s^{-1}$. At the length scale of the excursions of the particles from their potential minima and the distance between the two beads, the Reynolds number is small and therefore, we can describe the fluid motion around the beads in the Stokes limit. Consequently, the over-damped particle dynamics is described by the Langevin equations,

$$\dot{\mathbf{r}}_i = \mathbf{u}(\mathbf{r}_i) + \mathcal{H}_{ij}\mathbf{f}_j^V + \mathbf{f}_i^S \,, \tag{4}$$

with the four 3×3 mobility matrices

$$\mathcal{H}_{11} = \mathcal{H}_{22} = \frac{1}{\zeta}\mathcal{I} \,, \tag{5a}$$

$$\mathcal{H}_{12} = \mathcal{H}_{21} = \frac{1}{\zeta}\frac{3a}{4r_{12}}\left[\mathcal{I} + \frac{\mathbf{r}_{12} \otimes \mathbf{r}_{12}}{r_{12}^2}\right] \,, \tag{5b}$$

including the Stokes friction coefficient $\zeta = 6\pi\eta a$ for a single point-particle. [49]. The latter two matrices describe the hydrodynamic interaction between two point-particles in terms of the Oseen tensor [5] and $\mathcal{I}$ represents the unity matrix. The dyadic product (tensor product) $\otimes$ has been used as well as the distance vector $\mathbf{r}_{12} := \mathbf{r}_1 - \mathbf{r}_2$ between the beads, with $r_{12} = |\mathbf{r}_{12}|$.

The stochastic forces in the Langevin model have their origin in the velocity fluctuations of the surrounding liquid. In a quiescent fluid these random forces are uncorrelated along orthogonal directions in the bulk [50]. This assumption is kept in our Langevin model, because shear-induced cross-correlations between the stochastic forces along orthogonal directions are expected to be small [29, 51, 52]. So, for the contribution $\mathbf{f}_i^S(t)$ in eq. (4) we assume a zero mean and a vanishing correlation time [5]:

$$\langle\mathbf{f}_i^S(t)\rangle = 0 \,, \tag{6a}$$

$$\langle\mathbf{f}_i^S(t) \otimes \mathbf{f}_j^S(t')\rangle = 2k_BT\mathcal{H}_{ij}\delta(t - t') \,. \tag{6b}$$

The strength of the stochastic forces is proportional to the thermal energy k_BT.

The orientation of the connection vector between the potential minima, $\mathbf{q}_{12} := \mathbf{q}_1 - \mathbf{q}_2$, with respect to the flow direction is described by the angle ϕ. It has a strong influence on the correlation functions of the positional fluctuations of the particles. For this reason, we investigate three characteristic setups, where $\mathbf{q}_{12}$ is either parallel to the external flow $\mathbf{u}$ ($\phi = 0$), or perpendicular ($\phi = \pi/2$), or oblique ($\phi = \pi/4$) as sketched in fig. 1.

B. Solutions and relaxation times

There are two characteristic time scales in the system. One is determined by the inverse shear rate $\dot{\gamma}^{-1}$ and the other one is given by the relaxation time $\tau := \zeta/k$ of the particles in the two identical potentials. Their ratio gives the dimensionless Weissenberg number,

$$\mathrm{Wi} := \dot{\gamma}\tau \,, \tag{7}$$

which will be useful for the further discussion.

The first step in the solution of eq. (4) is to rewrite the equation of motion in a more compact form by introducing the positional vector $\mathbf{R} = (\mathbf{r}_1, \mathbf{r}_2)$ with six components and the 6×6 mobility matrix $\mathcal{H}$,

$$\mathcal{H} = \begin{pmatrix} \mathcal{H}_{11} & \mathcal{H}_{12} \\ \mathcal{H}_{12} & \mathcal{H}_{22} \end{pmatrix} \,, \tag{8}$$

composed of the sub-matrices $\mathcal{H}_{ij}$ from eqs. (5). The shear flow in eq. (3) can be written in an analogous manner with the 6×6 shear rate tensor $\mathcal{U}$,

$$\mathbf{U}(\mathbf{R}) = \mathcal{U}\mathbf{R} \,, \tag{9}$$

with $\mathcal{U}_{12} = \mathcal{U}_{45} = \dot{\gamma}$ and all other $\mathcal{U}_{kl} = 0$. The equation of motion (4) then takes the form,

$$\dot{\mathbf{R}} = \mathcal{U}\mathbf{R} + k\mathcal{H}(\mathbf{Q} - \mathbf{R}) + \mathbf{F} \,, \tag{10}$$

where the vector $\mathbf{Q} = (\mathbf{q}_1, \mathbf{q}_2)$ describes the positions of the two potential minima being separated by the distance d. The stochastic contribution $\mathbf{F}$ in eq. (10) is obtained from eqs. (6):

$$\langle\mathbf{F}(t)\rangle = 0 \,, \tag{11a}$$

$$\langle\mathbf{F}(t) \otimes \mathbf{F}(t')\rangle = 2k_BT\mathcal{H}\delta(t - t') \,. \tag{11b}$$

We assume two well separated point-particles with small values of a/d and small fluctuations around their mean positions, i.e. $k_BT/(ka^2) \ll 1$. The experimental results described in Ref. [34], which were obtained for $a/d \approx 1/4$ and a magnitude of the fluctuations below $a/10$, are well described within this approximation.

Since we investigate the particle fluctuations, the mean position $\mathbf{R}_\phi := \langle\mathbf{R}(t)\rangle$ has to be determined first. In the case $\phi = 0$ the mean positions are identical with the locations of the potential minima: $\mathbf{R}_0 = \mathbf{Q}$. For $\phi = \pi/2$ and $\phi = \pi/4$, $\mathbf{R}_\phi$ is obtained numerically by determining the stationary solution of eq. (10) in the absence of noise. Disregarding the hydrodynamic interaction between the two particles one finds the analytical expressions,

$$\mathbf{R}_{\pi/2}^a = \frac{d}{2}\left(\mathrm{Wi}, 1, 0, -\mathrm{Wi}, -1, 0\right) \,, \tag{12a}$$

$$\mathbf{R}_{\pi/4}^a = \frac{d}{4}\left(\sqrt{2} + \mathrm{Wi}, \sqrt{2}, 0, -\sqrt{2} - \mathrm{Wi}, -\sqrt{2}, 0\right) \,, \tag{12b}$$

which may serve as an approximation of the stationary solution and as the starting point of the numerical iteration.

The equation of motion for the particle fluctuations $\bar{\mathbf{R}} = (\bar{x}_1, \bar{y}_1, \bar{z}_1, \bar{x}_2, \bar{y}_2, \bar{z}_2)$ are obtained by the ansatz $\mathbf{R} = \mathbf{R}_\phi + \bar{\mathbf{R}}$ and the linearization of eq. (10) with respect to $\bar{\mathbf{R}}$:

$$\dot{\bar{\mathbf{R}}} = \mathcal{U}\bar{\mathbf{R}} - k\mathcal{H}\bar{\mathbf{R}} + k\left[\nabla\mathcal{H}\bar{\mathbf{R}}\right](\mathbf{Q} - \mathbf{R}_\phi) + \mathbf{F} \,. \tag{13}$$

Here the mobility matrix $\mathcal{H}$ and its derivative are evaluated at the exact mean positions $\mathbf{R}_\phi$. For $\phi = 0$

one has $\mathbf{R}_\phi = \mathbf{Q}$ and the third contribution on the right hand side vanishes. Introducing the matrix $\mathcal{K} := [\nabla \otimes (\mathcal{H}(\mathbf{Q} - \mathbf{R}_\phi))]^T$, eq. (13) can be rewritten to

$$\dot{\bar{\mathbf{R}}} = -(k\mathcal{H} - \mathcal{U} - k\mathcal{K})\bar{\mathbf{R}} + \mathbf{F} = -\mathcal{M}\bar{\mathbf{R}} + \mathbf{F}, \quad (14)$$

and this linear equation has the formal solution:

$$\bar{\mathbf{R}}(t) = e^{-t\mathcal{M}}\bar{\mathbf{R}}(0) + \int_0^t dt' e^{(t'-t)\mathcal{M}}\mathbf{F}. \quad (15)$$

By introducing the scaled deviation

$$\tilde{\mathbf{R}} = \frac{\bar{\mathbf{R}}}{\sqrt{B}}, \quad \text{with} \quad B = \frac{2k_BT}{k}, \quad (16)$$

and taking into account the statistical properties of the stochastic forces as given by eq. (11), one can determine by a straight-forward calculation, assisted by computer algebra, the correlation matrix $\mathcal{C}(t)$ defined by,

$$\mathcal{C}(t) := \langle \tilde{\mathbf{R}}(0) \otimes \tilde{\mathbf{R}}(t) \rangle \quad \text{for} \quad t \geq 0. \quad (17)$$

The brackets $\langle \cdot \rangle$ denote the ensemble average over a large number of particle trajectories. The elements $\mathcal{C}_{kl}(t)$ of the Matrix $\mathcal{C}(t)$ can be represented as a sum of six exponentially decaying contributions,

$$\mathcal{C}_{kl}(t) = \sum_\alpha g_{\alpha,kl} e^{-\lambda_\alpha t} \quad (\alpha, k, l = 1...6), \quad (18)$$

where the coefficients $g_{\alpha,kl}$ depend on the Weissenberg number $\mathrm{Wi} = \dot{\gamma}\tau$ and on the distance between the potential minima d.

The origin of the relaxation times $1/Re(\lambda_\alpha)$, given by the eigenvalues λ_α of the matrix $\mathcal{M} := k\mathcal{H} - \mathcal{U} - k\mathcal{K}$, can be explained as follows: After a stochastic kick that pushes the particles away from their mean positions, the potential forces start to pull them back. During this relaxation the particle motion can be decomposed into parallel or anti-parallel translations as illustrated in fig. 2. It is the hydrodynamic interaction between the particles, which accelerates or damps this process, since the resulting hydrodynamic forces depend on the relative particle motions. The beads relax faster, if they move in the same direction. The whole relaxation process is described by six relaxation rates, λ_α, two for each spatial direction and in the two cases $\phi = \pi/2$ and $\phi = \pi/4$ some of them may even be complex. For the configuration $\phi = 0$, cf. fig. 1 a), two relaxation modes coincide, so there are only four instead of six different relaxation times.

III. CORRELATION FUNCTIONS

In the two-particle system, the fluctuation statistics of one particle is influenced by its neighbor. We call
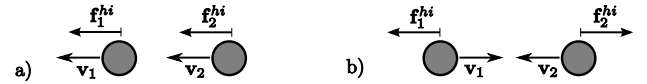

FIG. 2. The motion of particle 1 causes via the hydrodynamic interaction a force $\mathbf{f}_2^{hi}$ on particle 2 and vice versa. In part a), where the two particles move in the same direction, the resulting hydrodynamic forces accelerate the motion. This situation corresponds to the parallel relaxation. Part b) shows the anti-parallel case, where the forces $\mathbf{f}_i^{hi}$ decelerate the motion.

the corresponding correlation functions 'one-particle correlations' and for the inter-particle cross-correlations between the random displacements of two different particles we use the notation 'inter-particle correlations'.

In a previous study on hydrodynamic interactions between two trapped Brownian particles in a quiescent fluid, anti cross-correlations between their random motions along parallel spatial directions were found [6]. We show, that the shear flow alters these correlations and additionally induces inter-particle cross-correlations along orthogonal directions in the shear plane.

In this section the exact expressions and the approximations of the correlation functions $\mathcal{C}_{kl}(t)$, as defined by eq. (17), are discussed in detail and they are also compared with numerically obtained solutions of the Langevin equation (10). The behavior of $\mathcal{C}_{kl}(t)$ depends on the trap distance d, and in the limit $d \to \infty$, our formulas become identical to the recently presented results for a single trapped particle in a linear shear flow [33]. Since our results depend on the angle ϕ between the connection vector $\mathbf{q}_{12}$ and the flow direction the three characteristic configurations, as sketched in fig. 1, are analyzed.

A. Parallel case: $\phi = 0$

At first, we consider the two-particle configuration with the connection vector $\mathbf{q}_{12}$ parallel to the flow lines $\mathbf{u}$ as sketched in fig. 1 a), e.g. $\mathbf{Q} = d/2(1,0,0,-1,0,0)$. The discussion of the one-particle correlations in sect. III A 1 is complemented by the analysis of the inter-particle correlations in sect. III A 2.

Similar to the case of two trapped particles in a quiescent fluid in Ref. [6] there are four different relaxation rates describing the four relaxation times in the system, cf. sect. II B:

$$\lambda_1 = \frac{1+2\mu}{\tau}, \qquad \lambda_3 = \frac{1-2\mu}{\tau}, \quad (19a)$$

$$\lambda_2 = \frac{1+\mu}{\tau}, \qquad \lambda_4 = \frac{1-\mu}{\tau}. \quad (19b)$$

The parameter $0 < \mu := 3a/(4d) < 3/8$ is a measure for the distance between the traps. λ_1 and λ_3 correspond to the particle motions parallel and anti-parallel to the connection vector $\mathbf{q}_{12}$ (longitudinal displacements), while λ_2
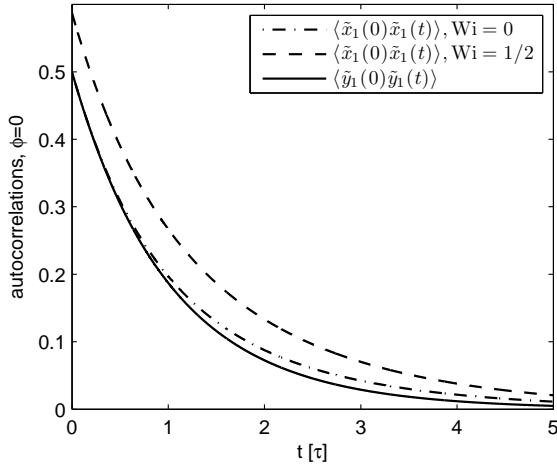
FIG. 3. The autocorrelations, $\langle \tilde{x}_1(0)\tilde{x}_1(t)\rangle = \langle \tilde{x}_2(0)\tilde{x}_2(t)\rangle$, along the flow direction are shown for Wi = 0 (dash-dotted line) and for Wi = 1/2 (dashed line). The correlation functions perpendicular to the flow direction, $\langle \tilde{y}_i(0)\tilde{y}_i(t)\rangle = \langle \tilde{z}_i(0)\tilde{z}_i(t)\rangle$ with $i = 1, 2$ (solid line), do not depend on the Weissenberg number. All curves are obtained for a distance $d = 4a$ and t is given in units of τ.

and λ_4 belong to the particle relaxations perpendicular to $\mathbf{q}_{12}$ (transversal displacements).

1. One-particle correlations

The autocorrelations are identical for both particles but they are different for the longitudinal and transversal displacements: $\langle \tilde{x}_1(0)\tilde{x}_1(t)\rangle = \langle \tilde{x}_2(0)\tilde{x}_2(t)\rangle$ and $\langle \tilde{y}_1(0)\tilde{y}_1(t)\rangle = \langle \tilde{y}_2(0)\tilde{y}_2(t)\rangle = \langle \tilde{z}_1(0)\tilde{z}_1(t)\rangle = \langle \tilde{z}_2(0)\tilde{z}_2(t)\rangle$. The expressions

$$\langle \tilde{x}_1(0)\tilde{x}_1(t)\rangle = \frac{1}{4}\left(e^{-\lambda_1 t} + e^{-\lambda_3 t}\right)$$
$$+ \frac{\text{Wi}^2}{4\mu}\left(\frac{-(1+\mu)e^{-\lambda_1 t}}{6\mu^2 + 7\mu + 2} + \frac{e^{-\lambda_2 t}}{2 + 3\mu}\right)$$
$$+ \frac{\text{Wi}^2}{4\mu}\left(\frac{(1-\mu)e^{-\lambda_3 t}}{6\mu^2 - 7\mu + 2} - \frac{e^{-\lambda_4 t}}{2 - 3\mu}\right), \quad (20a)$$

$$\langle \tilde{y}_1(0)\tilde{y}_1(t)\rangle = \langle \tilde{z}_1(0)\tilde{z}_1(t)\rangle = \frac{1}{4}\left(e^{-\lambda_2 t} + e^{-\lambda_4 t}\right), \quad (20b)$$

are exponentially decaying in time and both functions are plotted in fig. 3 for different values of the Weissenberg number Wi. Due to the scaling (16) the value of $\langle \tilde{y}_1(0)\tilde{y}_1(0)\rangle$ is 1/2. The correlation functions (20) depend via μ on the trap distance d, which leads to interesting corrections to the autocorrelations compared to the case of one isolated particle in Ref. [33].

The distinct relaxation rates given by eqs. (19) lead to different autocorrelations of particle displacements along and perpendicular to $\mathbf{q}_{12}$, independent of the parameter Wi. This is also indicated in fig. 3 by the difference
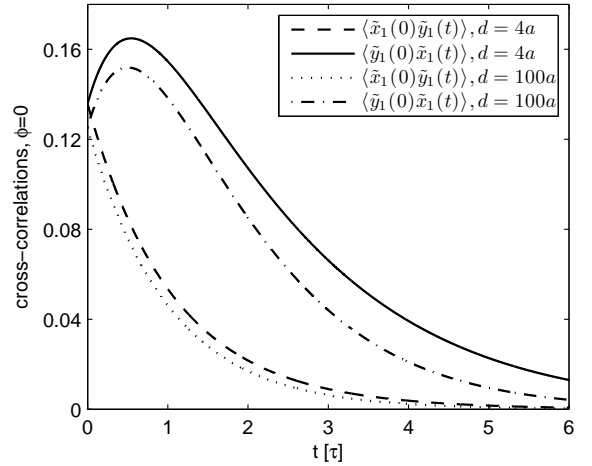

FIG. 4. Shear-induced cross-correlations of a single particle in the parallel case for Wi = 1/2 and $d = 4a$ respectively $d = 100a$. $\langle \tilde{x}_1(t)\tilde{y}_1(0)\rangle$ has a maximum around $t' \approx \tau$, which does not depend on Wi and only very weakly on d.

between the correlations $\langle \tilde{x}_1(0)\tilde{x}_1(t)\rangle$ (dash-dotted line) and $\langle \tilde{y}_1(0)\tilde{y}_1(t)\rangle$ (solid line). The latter one is independent of the Weissenberg number, which is similar to the case of an isolated trapped particle, where only the autocorrelation in flow direction (20a) depends on Wi^2 [33].

Any translation of a particle in y direction is coupled via the flow profile (3) to a change of the particle's velocity in x direction, which leads to a change of the particle's positional fluctuation along the x direction. Consequently, the particle fluctuations in the x and y directions become correlated due to the shear flow. The resulting cross-correlations between the displacements along orthogonal directions in the shear plane are linear functions of the parameter Wi, similar to the single particle case in Refs. [33, 34]. However, compared to these results, we obtain for the two-particle system an additional dependence on the trap distance d. The time-dependence of the cross-correlations is given by the following expressions:

$$\langle \tilde{x}_1(0)\tilde{y}_1(t)\rangle = \frac{\text{Wi}}{4}\left(\frac{e^{-\lambda_2 t}}{2 + 3\mu} + \frac{e^{-\lambda_4 t}}{2 - 3\mu}\right), \quad (21a)$$

$$\langle \tilde{y}_1(0)\tilde{x}_1(t)\rangle = \frac{\text{Wi}}{4\mu}\left(e^{-\lambda_2 t} - e^{-\lambda_4 t}\right)$$
$$+ \frac{\text{Wi}}{2\mu}\left(\frac{(1-\mu)e^{-\lambda_3 t}}{2 - 3\mu} - \frac{(1+\mu)e^{-\lambda_1 t}}{2 + 3\mu}\right). \quad (21b)$$

Both functions are plotted in fig. 4 for two different distances. The two sets of curves indicate that the magnitude of the cross-correlation increases weakly with decreasing values of d. The cross-correlation functions involving the z coordinate vanish as in Ref. [33].

The time-asymmetry of the shear-induced cross-correlations, namely $\langle \tilde{y}_1(0)\tilde{x}_1(t)\rangle \neq \langle \tilde{x}_1(0)\tilde{y}_1(t)\rangle$ with $t > 0$, can be explained in the following way: A random particle

displacement at $t = 0$ in y direction leads immediately after the kick to a linear growth of the particle's x coordinate due to the larger flow velocity $\mathbf{u}(\mathbf{r})$ at a larger value of the y coordinate. Consequently, for small values of t, the product $\tilde{y}_1(0)\tilde{x}_1(t)$ grows in time until the particle is pulled back by the linear spring force, which happens on the time scale $\tau = \zeta/k$. The result is a maximum in the correlation function $\langle \tilde{y}_1(0)\tilde{x}_1(t) \rangle$ at a time of the order of τ. Considering the effect of a random kick in x direction at $t = 0$, the particle does not jump between streamlines of different velocity and therefore the cross-correlation $\langle \tilde{x}_1(0)\tilde{y}_1(t) \rangle$ does not show this maximum and decays exponentially.

By replacing the time t by $-t$ in eq. (21a) the two functions (21a) and (21b) can be combined to one correlation function $\langle \tilde{x}_1(0)\tilde{y}_1(t) \rangle$, where t can now take positive and negative values. This function is asymmetric with respect to time-reflections $t \rightarrow -t$. A similar behavior was previously found for the fluctuations of the fluid-velocity in a shear flow [28].

The static correlation functions given by eqs. (20a) – (21b) for $t = 0$ determine also the positional distribution function $P(\mathbf{r})$ of a Brownian particle in a potential as described in more detail in Ref. [33]. It is an interesting question, how the single particle distribution in a shear flow is changed by the presence of a second one.

In a linear shear flow $P(\mathbf{r})$ has an elliptical shape in the shear plane and the angle θ between the major axis of the ellipse and the flow direction is determined by the equation

$$\tan\theta = \frac{1}{2}\left[\frac{\langle \tilde{x}_1\tilde{y}_1 \rangle}{|\langle \tilde{x}_1\tilde{y}_1 \rangle|}\sqrt{4 + G^2} - G \right], \qquad (22)$$

$$\text{with} \qquad G = \frac{\langle \tilde{x}_1^2 \rangle - \langle \tilde{y}_1^2 \rangle}{\langle \tilde{x}_1\tilde{y}_1 \rangle}. \qquad (23)$$

Using the d-dependent static correlations from eqs. (20) and (21) we obtain

$$G = \text{Wi}\, \frac{1 + 3\mu^2}{1 - 4\mu^2}. \qquad (24)$$

Consequently the inclination angle θ is a function of the parameter d too. In fig. 5 $\tan(\theta)$ is shown as a function of $\mu = 3a/(4d)$ for three different values of the Weissenberg number Wi and in all three cases $\tan(\theta)$ decreases considerably when the two particles approach. Since θ changes in the same manner by decreasing d or increasing Wi, the shear-flow effects can be considered to be amplified by the presence of the second particle.

2. Inter-particle correlations

The motion of the two trapped Brownian particles is coupled via the hydrodynamic interaction. In a quiescent fluid this coupling leads to a cross-correlation between the thermal fluctuations of the two particles along the
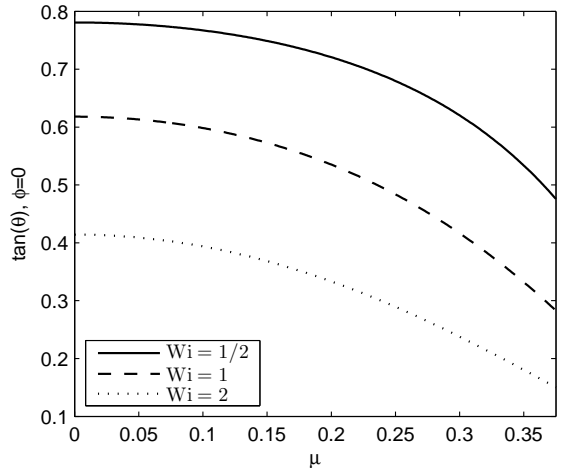

FIG. 5. The inclination angle θ of the single particle distribution is shown as function of $\mu = 3a/(4d)$ for three different values of the Weissenberg number Wi.

same direction [6]. Since this cross-correlation is negative as a function of time, cf. fig. 6, the notion 'anti cross-correlation' is used. For the anti cross-correlation of the longitudinal displacements we obtain a shear-induced correction, similar as for the one-particle autocorrelation in eq. (20a), which is proportional to Wi^2:

$$\langle \tilde{x}_1(0)\tilde{x}_2(t) \rangle = \frac{1}{4}\left(e^{-\lambda_1 t} - e^{-\lambda_3 t} \right)$$
$$+ \frac{\text{Wi}^2}{4\mu}\left(\frac{-(1+\mu)e^{-\lambda_1 t}}{6\mu^2 + 7\mu + 2} + \frac{e^{-\lambda_2 t}}{2 + 3\mu} \right),$$
$$+ \frac{\text{Wi}^2}{4\mu}\left(\frac{-(1-\mu)e^{-\lambda_3 t}}{6\mu^2 - 7\mu + 2} + \frac{e^{-\lambda_4 t}}{2 - 3\mu} \right). \qquad (25)$$

The cross-correlations between random particle-displacements perpendicular to $\mathbf{q}_{12}$ are independent of the Weissenberg number Wi:

$$\langle \tilde{y}_1(0)\tilde{y}_2(t) \rangle = \langle \tilde{z}_1(0)\tilde{z}_2(t) \rangle = \frac{1}{4}\left(e^{-\lambda_2 t} - e^{-\lambda_4 t} \right). \qquad (26)$$

Both correlation functions are plotted in fig. 6.

As indicated in fig. 2, the relaxation processes of the displacements of the two particles along the same spatial direction can be decomposed into a parallel and an anti-parallel translation. In the present case the eigenvalue λ_1 (λ_2) in eqs. (19) corresponds to the parallel relaxation modes along (perpendicular to) the connection vector $\mathbf{q}_{12}$. For the parallel motions, the signs of the particle displacements are always equal for both particles ($+, +$ or $-, -$), whereas for the anti-parallel ones the corresponding displacements have opposite signs ($+, -$ or $-, +$). As a consequence the product of the two displacements is always positive for the parallel case and negative for the anti-parallel case, as indicated by the prefactors of the corresponding contributions in the correlation functions
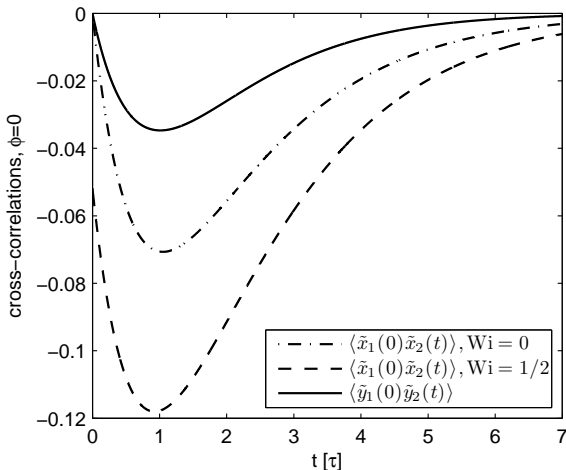
FIG. 6. The cross-correlation functions between the two beads along parallel directions are shown for $\phi = 0$ and $d = 4a$. The minimum of $\langle \tilde{x}_1(0)\tilde{x}_2(t)\rangle = \langle \tilde{x}_2(0)\tilde{x}_1(t)\rangle$ increases with the Weissenberg number Wi and is always deeper than the one of the function $\langle \tilde{y}_1(0)\tilde{y}_2(t)\rangle = \langle \tilde{z}_1(0)\tilde{z}_2(t)\rangle$, which is independent of Wi.

in eq. (25) and eq. (26). As the magnitudes of the anti-parallel translations are larger than the parallel ones, the superposition of the two different modes is negative and has a pronounced minimum at a time $t' \approx \tau$, as shown in fig. 6. The value of t' in case of eq. (25) depends only weakly on the distance d between the two traps. For the cross-correlation $\langle \tilde{y}_1(0)\tilde{y}_2(t)\rangle$ an analytical expression for t' and its magnitude can be given:

$$t' = \frac{\tau}{2\mu} \ln\left(\frac{1+\mu}{1-\mu}\right), \qquad (27)$$

$$\langle \tilde{y}_1(0)\tilde{y}_2(t')\rangle = \frac{1}{4}\left(\left(\frac{1-\mu}{1+\mu}\right)^{\frac{1+\mu}{2\mu}} - \left(\frac{1-\mu}{1+\mu}\right)^{\frac{1-\mu}{2\mu}}\right). \quad (28)$$

For finite values of the Weissenberg number Wi the cross-correlation of the longitudinal displacements, $\langle \tilde{x}_1(0)\tilde{x}_2(t)\rangle$, also includes contributions describing relaxation processes perpendicular to $\mathbf{q}_{12}$ with the eigenvalues λ_2 and λ_4. These additional contributions cause larger shear-induced corrections to the cross-correlation in eq. (25) than for the autocorrelation function in eq. (20a), which can be seen by comparing the deviations between the dashed-dotted and the dashed curves in fig. 3 and in fig. 6.

For a single particle in a linear shear flow shear-induced cross-correlations between displacements along perpendicular directions in the shear plane were found, which are proportional to the Weissenberg number [33]. In the two-particle system, one also obtains cross-correlations between the displacements of two different particles along orthogonal directions in the shear plane as described by:
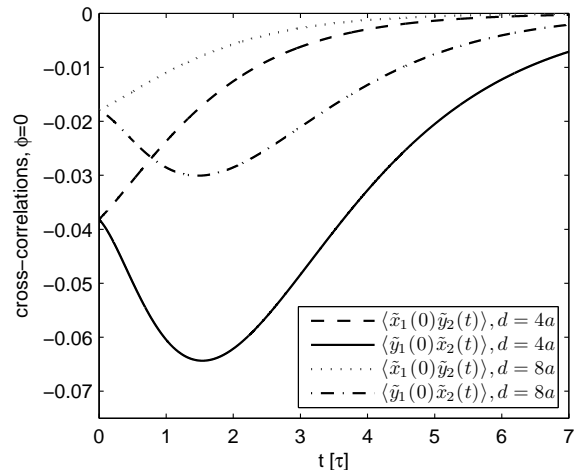

FIG. 7. Shear-induced cross-correlations between orthogonal fluctuations of different particles in the case, where $\mathbf{q}_{12}$ is parallel to the streamlines, for Wi $= 1/2$ and different distances.

$$\langle \tilde{x}_1(0)\tilde{y}_2(t)\rangle = \frac{\text{Wi}}{4}\left(\frac{e^{-\lambda_2 t}}{2+3\mu} - \frac{e^{-\lambda_4 t}}{2-3\mu}\right), \qquad (29a)$$

$$\langle \tilde{y}_2(0)\tilde{x}_1(t)\rangle = \frac{\text{Wi}}{4\mu}\left(e^{-\lambda_2 t} + e^{-\lambda_4 t}\right)$$
$$- \frac{\text{Wi}}{2\mu}\left(\frac{(1+\mu)e^{-\lambda_1 t}}{2+3\mu} + \frac{(1-\mu)e^{-\lambda_3 t}}{2-3\mu}\right). \quad (29b)$$

Both functions are plotted for different values of the trap distance in fig. 7 and one can see that the magnitudes of the correlations are larger for smaller values of d. Note that in general the particle index in the previous equations can be interchanged: $\langle \tilde{x}_1(0)\tilde{y}_2(t)\rangle = \langle \tilde{x}_2(0)\tilde{y}_1(t)\rangle$.

The ratio between the two shear-induced cross-correlations at $t = 0$ is independent of the Weissenberg number Wi and given by:

$$\frac{\langle \tilde{x}_1(0)\tilde{y}_2(0)\rangle}{\langle \tilde{x}_1(0)\tilde{y}_1(0)\rangle} = \frac{-3\mu}{2} = \frac{-9a}{8d}. \qquad (30)$$

This relation is reasonable for a sufficiently large ratio d/a. It might serve in an experiment as a consistency check, since the bead radius a and the particle distance d are usually well known. If the two beads come close to each other, additional effects related to their shear-induced rotation may come into play. This is in general a limitation of our Langevin model (4) for point-like particles with an effective hydrodynamic radius. In Ref. [7] particle rotations caused by an external torque have been taken into account in a Langevin model for two trapped particles in a quiescent fluid. This work describes a coupling between translational and rotational particle motions, which was confirmed by experiments [53].

The asymmetry in eqs. (29) with respect to time, $t \to -t$, has a similar origin as explained above for the

shear-induced one-particle correlations (21). The location of the minimum is again mainly determined by the relaxation time τ of the beads in the harmonic potentials.

Note, that for all described correlation functions the single particle case is recovered in the limit $d \to \infty$, which corresponds to $\mu \to 0$, for example:

$$\lim_{\mu \to 0} \langle \tilde{y}_1(0)\tilde{x}_1(t) \rangle = \frac{\text{Wi}}{4}\left(1 + 2\frac{t}{\tau}\right)e^{-t/\tau}. \qquad (31)$$

All the correlation functions presented in this subsection have already been measured in experiments [34, 54].

B. Perpendicular case: $\phi = \pi/2$

For $\phi = \pi/2$ the time-dependence of the correlation functions and their magnitudes are changed compared to the parallel orientation $\phi = 0$. This subsection focuses on these differences.

The formulas (19) for the eigenvalues of the matrix $\mathcal{M}$ were derived for the identity $\mathbf{R}_0 = \mathbf{Q}$. This allows the determination of exact analytical formulas for the correlations. In the present case, $\mathbf{R}_{\pi/2}$ has to be determined numerically as well as the relaxation rates λ_i and the exact functions $\mathcal{C}_{kl}(t)$. However, if we use the approximation $\mathbf{R}_{\pi/2} = \mathbf{Q} = d/2(0, 1, 0, 0, -1, 0)$, which is valid for small Weissenberg numbers, we obtain analytical formulas for the correlations that also describe quantitatively the characteristics of the functions $\mathcal{C}_{kl}(t)$ at large values of Wi. Within this assumption eqs. (19) remain, but the eigenvalues exchange their meanings: Now λ_1 and λ_3 belong to the longitudinal fluctuations in the y direction, whereas λ_2 and λ_4 describe the transversal motions in x and z direction, perpendicular to $\mathbf{q}_{12}$. We also compare the numerical solutions with direct simulations of the Langevin equation (4).

1. One-particle correlation

For the perpendicular configuration the one-particle autocorrelations are given for the approximation $\mathbf{R}_{\pi/2} = \mathbf{Q}$ by the following expressions:

$$\langle \tilde{x}_1(0)\tilde{x}_1(t) \rangle = \frac{1}{4}\left(e^{-\lambda_2 t} + e^{-\lambda_4 t}\right)$$
$$+ \frac{\text{Wi}^2}{4\mu}\left(\frac{(2\mu - 1)\,e^{-\lambda_4 t}}{3\mu^2 - 5\mu + 2} + \frac{e^{-\lambda_3 t}}{2 - 3\mu}\right)$$
$$+ \frac{\text{Wi}^2}{4\mu}\left(\frac{(2\mu + 1)e^{-\lambda_2 t}}{3\mu^2 + 5\mu + 2} - \frac{e^{-\lambda_1 t}}{2 + 3\mu}\right), \qquad (32a)$$

$$\langle \tilde{y}_1(0)\tilde{y}_1(t) \rangle = \frac{1}{4}\left(e^{-\lambda_1 t} + e^{-\lambda_3 t}\right), \qquad (32b)$$

$$\langle \tilde{z}_1(0)\tilde{z}_1(t) \rangle = \frac{1}{4}\left(e^{-\lambda_2 t} + e^{-\lambda_4 t}\right). \qquad (32c)$$

While the correlations $\langle \tilde{y}_1(0)\tilde{y}_1(t) \rangle$ and $\langle \tilde{z}_1(0)\tilde{z}_1(t) \rangle$ of the displacements perpendicular to the flow lines were identical in the case $\phi = 0$, they are different in the present
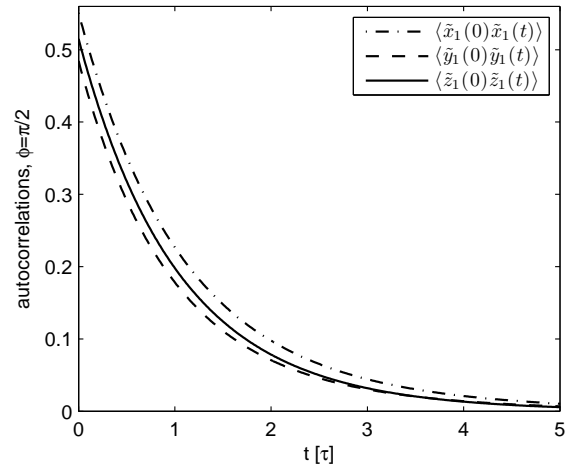

FIG. 8. Autocorrelations for $\phi = \pi/2$, $d = 4a$ and Wi $= 1/2$. $\langle \tilde{x}_1(0)\tilde{x}_1(t) \rangle$, $\langle \tilde{y}_1(0)\tilde{y}_1(t) \rangle$ and $\langle \tilde{z}_1(0)\tilde{z}_1(t) \rangle$ are different, because of the different relaxation rates and additional Wi^2-contributions in x direction. One has $\langle \tilde{x}_1(0)\tilde{x}_1(t) \rangle = \langle \tilde{z}_1(0)\tilde{z}_1(t) \rangle$ only for Wi $= 0$.

case, because they describe positional fluctuations either parallel or perpendicular to $\mathbf{q}_{12}$. Only for a vanishing Weissenberg number one obtains $\langle \tilde{x}_1(0)\tilde{x}_1(t) \rangle = \langle \tilde{z}_1(0)\tilde{z}_1(t) \rangle$, but for a finite shear rate the correlation functions are all different – for the approximations in eqs. (32) as well as for the numerical solutions shown in fig. 8.

The shear-induced cross-correlations between particle displacements along orthogonal directions in the shear plane behave qualitatively similar as in the case $\phi = 0$. For the approximation $\mathbf{R}_{\pi/2} = \mathbf{Q}$ they are described by the formulas

$$\langle \tilde{x}_1(0)\tilde{y}_1(t) \rangle = \frac{\text{Wi}}{4}\left(\frac{e^{-\lambda_1 t}}{2 + 3\mu} + \frac{e^{-\lambda_3 t}}{2 - 3\mu}\right), \qquad (33a)$$

$$\langle \tilde{y}_1(0)\tilde{x}_1(t) \rangle = \frac{\text{Wi}}{4\mu}\left(e^{-\lambda_3 t} - e^{-\lambda_1 t}\right)$$
$$+ \frac{\text{Wi}}{2\mu}\left(\frac{(1 + 2\mu)e^{-\lambda_2 t}}{2 + 3\mu} - \frac{(1 - 2\mu)e^{-\lambda_4 t}}{2 - 3\mu}\right). \qquad (33b)$$

The magnitudes of the different contributions in eqs. (33) changed compared to the expressions in eqs. (21), which influences the positional probability distribution $P(\mathbf{r})$ of one particle. The dependence of the inclination angle θ on the distance d is weaker in the present case than for $\phi = 0$, see fig. 13 in the next section. Possible consequences of this difference for the dynamics of beads-spring models for polymers in shear flows are discussed in the concluding remarks.

The magnitudes of the correlations functions given by eqs. (33) are smaller than those determined numerically for the exact distance $\mathbf{R}_{\pi/2}$, which are plotted in fig. 9. In the same figure these exact solutions are compared with
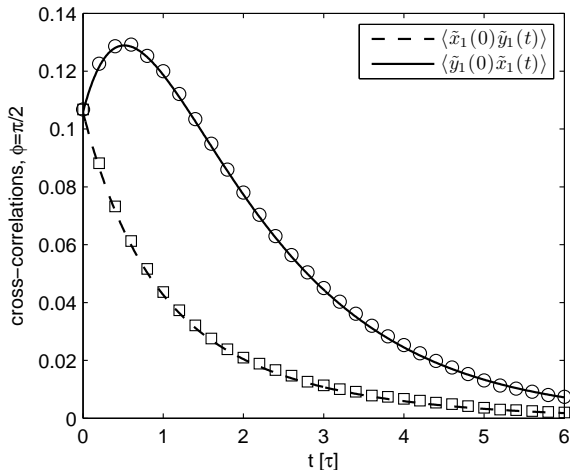
FIG. 9. Comparison of the numerically determined one-particle cross-correlations (lines) with the results from the direct simulation of eq. (4) (circles, squares). The error bars are smaller than the symbols. Parameters: $d = 4a$, Wi $= 1/2$.

FIG. 10. Inter-particle cross-correlations in the orthogonal case for $d = 4a$ and Wi $= 1/2$. $\langle \tilde{x}_1(0)\tilde{x}_2(t)\rangle$, $\langle \tilde{y}_1(0)\tilde{y}_2(t)\rangle$ and $\langle \tilde{z}_1(0)\tilde{z}_2(t)\rangle$ are all different and anti-correlated with pronounced minima. One obtains $\langle \tilde{x}_1(0)\tilde{x}_2(t)\rangle = \langle \tilde{z}_1(0)\tilde{z}_2(t)\rangle$ for Wi $= 0$.

the results of a Brownian dynamics simulation of eq. (4), where $2*10^6$ ensemble averages were made. This example illustrates the good agreement between both approaches, which is not affected by the choice of the Rotne-Prager tensor instead of the Oseen tensor in the simulation. The analytical expressions (33) turn out to be a good approximation for the parameters $d \geq 8a$ and Wi ≤ 0.1. Especially for smaller values of the trap distance d deviations in the relaxation times occur.

2. Inter-particle correlations

The cross-correlations of the random displacements between the two particles in the same direction are given for $\mathbf{R}_{\pi/2} = \mathbf{Q}$ by:

$$\langle \tilde{x}_1(0)\tilde{x}_2(t)\rangle = \frac{1}{4}\left(e^{-\lambda_2 t} - e^{-\lambda_4 t}\right)$$
$$+ \frac{\text{Wi}^2}{4\mu}\left(\frac{(1-2\mu)e^{-\lambda_4 t}}{3\mu^2 - 5\mu + 2} - \frac{e^{-\lambda_3 t}}{2 - 3\mu}\right)$$
$$+ \frac{\text{Wi}^2}{4\mu}\left(\frac{(1+2\mu)e^{-\lambda_2 t}}{3\mu^2 + 5\mu + 2} - \frac{e^{-\lambda_1 t}}{2 + 3\mu}\right), \quad (34a)$$

$$\langle \tilde{y}_1(0)\tilde{y}_2(t)\rangle = \frac{1}{4}\left(e^{-\lambda_1 t} - e^{-\lambda_3 t}\right), \quad (34b)$$

$$\langle \tilde{z}_1(0)\tilde{z}_2(t)\rangle = \frac{1}{4}\left(e^{-\lambda_2 t} - e^{-\lambda_4 t}\right). \quad (34c)$$

Similar to the one-particle correlations in sect. III B 1 and in contrast to the case $\phi = 0$ in sect. III A 2, all three correlation functions are different for finite values of the Weissenberg number. This is indicated by the expression in eqs. (34) as well as by the numerical correlation functions displayed in fig. 10, and they are again
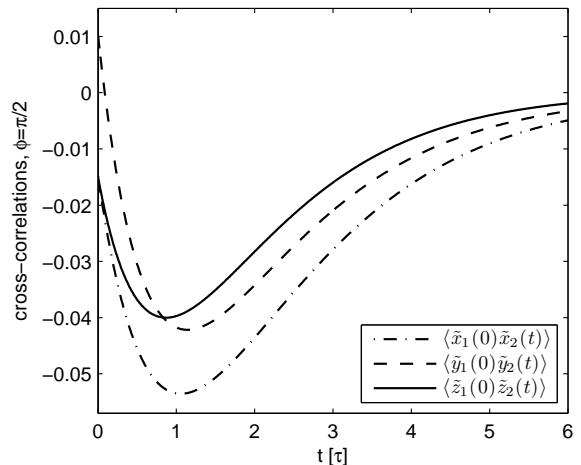
all anti-correlated.

The most striking difference between the case $\phi = 0$ and $\phi = \pi/2$ is found by looking at the shear-induced inter-particle correlations between orthogonal directions in the shear plane, which are given for $\mathbf{R}_{\pi/2} = \mathbf{Q}$ by the following expressions:

$$\langle \tilde{x}_1(0)\tilde{y}_2(t)\rangle = \frac{\text{Wi}}{4}\left(\frac{e^{-\lambda_1 t}}{2 + 3\mu} - \frac{e^{-\lambda_3 t}}{2 - 3\mu}\right), \quad (35a)$$

$$\langle \tilde{y}_1(0)\tilde{x}_2(t)\rangle = \frac{-\text{Wi}}{4\mu}\left(e^{-\lambda_1 t} + e^{-\lambda_3 t}\right)$$
$$+ \frac{\text{Wi}}{2\mu}\left(\frac{(1+2\mu)e^{-\lambda_2 t}}{2 + 3\mu} + \frac{(1-2\mu)e^{-\lambda_4 t}}{2 - 3\mu}\right). \quad (35b)$$

A Taylor expansion of the correlation function $\langle \tilde{y}_1(0)\tilde{x}_2(t)\rangle$ with respect to small values of μ reveals the difference between the parallel and the perpendicular orientations. For $\phi = 0$ one obtains up to the linear order of μ,

$$\langle \tilde{y}_1(0)\tilde{x}_2(t)\rangle \sim \mu\left(3 + 4\frac{t}{\tau} + 6\frac{t^2}{\tau^2}\right)e^{-t/\tau}, \quad (36)$$

whereas for $\phi = \pi/2$ one obtains,

$$\langle \tilde{y}_1(0)\tilde{x}_2(t)\rangle \sim \mu\left(3 + 2\frac{t}{\tau} + 6\frac{t^2}{\tau^2}\right)e^{-t/\tau}. \quad (37)$$

The first expression has only *one* extremum as a function of time. The different prefactor of $te^{-t/\tau}$ in the second expression is the origin of an additional extremum in the case $\phi = \pi/2$.

For $\mathbf{Q} = d/2(0, 1, 0, 0, -1, 0)$ the angle between the vector connecting the resulting mean positions of the particles, $\langle \mathbf{r}_{12}\rangle$, and the y axis increases as a function of Wi. In
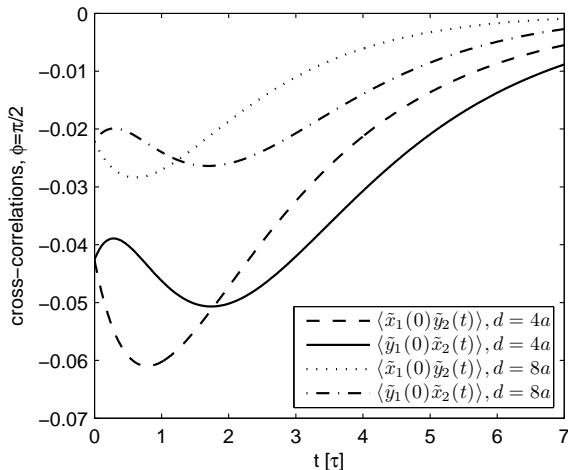
FIG. 11. Shear-induced inter-particle correlations in case of a tilted trap for a Weissenberg number $\mathrm{Wi} = 1/2$ and for the two distances $d = 4a$ and $d = 8a$. The time-dependence is different from the case $\phi = 0$, cf. Fig. 7.

this configuration the numerical solution for $\langle \tilde{y}_1(0)\tilde{x}_2(t)\rangle$ does not show a second extremum. However, if $\mathbf{Q}$ is tilted against the flow direction, like

$$\mathbf{Q} = \frac{d}{2\sqrt{1+\mathrm{Wi}^2}}(-\mathrm{Wi}, 1, 0, \mathrm{Wi}, -1, 0), \qquad (38)$$

the resulting vector $\langle \mathbf{r}_{12}\rangle$ becomes nearly parallel to the y axis and the second extremum of $\langle \tilde{y}_1(0)\tilde{x}_2(t)\rangle$ is obtained again, as predicted by the approximation in eq. (37). The result for the tilted trap is shown in fig. 11 for two different values of d. Moreover, the extrema are now stronger pronounced than predicted by eq. (37). Comparing this with fig. 7, where the results for $\phi = 0$ are plotted, it can be clearly seen, that the correlation $\langle \tilde{y}_1(0)\tilde{x}_2(t)\rangle$ now has an additional local maximum, cf. solid and dash-dotted line in fig. 7, and that $\langle \tilde{x}_1(0)\tilde{y}_2(t)\rangle$ has a minimum at small values of the time t, cf. dashed and dotted lines in fig. 7.

C. Oblique case: $\phi = \pi/4$

If the connection vector $\mathbf{q}_{12}$ between the two potential minima is oblique to the flow direction, further aspects for the correlation functions may come into play. In principle, the matrix $\mathcal{C}_{kl}(t)$ can be calculated for any angle ϕ. However, we focus on the special case $\phi = \pi/4$ as an example. This has the advantage that analytical expressions can be obtained under the assumption $\mathbf{R}_{\pi/4} = \mathbf{Q}$. These approximate solutions remain rather compact and may serve as a guide for the qualitative behavior of the correlation functions.

Since the linear shear flow (3) dictates a preferred direction in the system, the particle fluctuations are decom-

posed into eigenmodes parallel and perpendicular to the x axis as described in sect. II B. That's why in the oblique configuration the longitudinal displacements consist of a superposition of the eigenmodes in the shear plane. If $\phi = \pi/4$, the eigenvalues of the matrix $\mathcal{M}$ are given for $\mathbf{R}_{\pi/4} = \mathbf{Q} = d\sqrt{2}/4(1, 1, 0, -1, -1, 0)$ by the following expressions,

$$\lambda_1 = \frac{2 + 3\mu + \sqrt{\mu^2 - 2\mu\mathrm{Wi}}}{2\tau}, \qquad (39\mathrm{a})$$

$$\lambda_2 = \frac{2 + 3\mu - \sqrt{\mu^2 - 2\mu\mathrm{Wi}}}{2\tau}, \qquad (39\mathrm{b})$$

$$\lambda_3 = \frac{1 + \mu}{\tau}, \qquad (39\mathrm{c})$$

$$\lambda_4 = \frac{2 - 3\mu - \sqrt{\mu^2 + 2\mu\mathrm{Wi}}}{2\tau}, \qquad (39\mathrm{d})$$

$$\lambda_5 = \frac{2 - 3\mu + \sqrt{\mu^2 + 2\mu\mathrm{Wi}}}{2\tau}, \qquad (39\mathrm{e})$$

$$\lambda_6 = \frac{1 - \mu}{\tau}. \qquad (39\mathrm{f})$$

While λ_1 and λ_4 describe the parallel and anti-parallel relaxation modes in the x direction, λ_2 and λ_5 belong to the y direction, and λ_3 and λ_6 to the z direction. In contrast to the parallel case, the relaxation processes along the x and y direction in the shear plane are now affected by the shear rate. So the corresponding eigenvalues depend directly on the Weissenberg number. This was not the case in the previous section for $\mathbf{R}_{\pi/2} = \mathbf{Q}$. As long as $\mathrm{Wi} \neq 0$, the six relaxation parameters are different and can partly become complex numbers, causing oscillatory contributions to the functions $\mathcal{C}_{kl}(t)$.

In order to write down the full expressions for the correlations in a compact form, we introduce the following notions similar to eq. (18):

$$g_{1,1} = \mu + \frac{\mathrm{Wi}(\lambda_1 - \lambda_2)}{2\lambda_1}, \qquad (40\mathrm{a})$$

$$g_{2,1} = \mu - \frac{\mathrm{Wi}(\lambda_1 - \lambda_2)}{2\lambda_2}, \qquad (40\mathrm{b})$$

$$g_{4,1} = \mu + \frac{\mathrm{Wi}(\lambda_5 - \lambda_4)}{2\lambda_4}, \qquad (40\mathrm{c})$$

$$g_{5,1} = \mu - \frac{\mathrm{Wi}(\lambda_5 - \lambda_4)}{2\lambda_5}, \qquad (40\mathrm{d})$$

$$g_{1,2} = \mu - \frac{\mathrm{Wi}(3\lambda_1 + \lambda_2)}{2\lambda_1}, \qquad (40\mathrm{e})$$

$$g_{2,2} = \mu - \frac{\mathrm{Wi}(3\lambda_2 + \lambda_1)}{2\lambda_2}, \qquad (40\mathrm{f})$$

$$g_{4,2} = \mu + \frac{\mathrm{Wi}(3\lambda_4 + \lambda_5)}{2\lambda_4}, \qquad (40\mathrm{g})$$

$$g_{5,2} = \mu + \frac{\mathrm{Wi}(3\lambda_5 + \lambda_4)}{2\lambda_5}. \qquad (40\mathrm{h})$$

Analogous to the previous subsections we discuss the one-particle correlations first. The autocorrelations of a single particle show the same behavior as in the case

$\phi = \pi/2$. They are different in distinct directions as long as Wi $\neq 0$ and decay exponentially in time. For $\mathbf{R}_{\pi/4} = \mathbf{Q}$ the analytical formulas read

$$\langle \tilde{x}_1(0)\tilde{x}_1(t)\rangle = \frac{g_{1,1}e^{-\lambda_1 t}}{8\mu} + \frac{g_{2,1}e^{-\lambda_2 t}}{8\mu}$$
$$+ \frac{g_{4,1}e^{-\lambda_4 t}}{8\mu} + \frac{g_{5,1}e^{-\lambda_5 t}}{8\mu}, \tag{41a}$$

$$\langle \tilde{y}_1(0)\tilde{y}_1(t)\rangle = \frac{g_{1,2}e^{-\lambda_1 t}}{8(\mu - 2\mathrm{Wi})} + \frac{g_{2,2}e^{-\lambda_2 t}}{8(\mu - 2\mathrm{Wi})}$$
$$+ \frac{g_{4,2}e^{-\lambda_4 t}}{8(\mu + 2\mathrm{Wi})} + \frac{g_{5,2}e^{-\lambda_5 t}}{8(\mu + 2\mathrm{Wi})}, \tag{41b}$$

$$\langle \tilde{z}_1(0)\tilde{z}_1(t)\rangle = \frac{1}{4}\left(e^{-\lambda_3 t} + e^{-\lambda_6 t}\right). \tag{41c}$$

However, in contrast to eqs. (32) one can see that the two autocorrelation functions for the particle displacements in the shear plane, namely $\langle \tilde{x}_1(0)\tilde{x}_1(t)\rangle$ and $\langle \tilde{y}_1(0)\tilde{y}_1(t)\rangle$, include the four corresponding relaxation modes and depend in a complex way on the Weissenberg number.

The one-particle cross-correlations between orthogonal positional fluctuations in the shear plane, like $\langle \tilde{x}_1(0)\tilde{y}_1(t)\rangle$, are purely shear-induced in the parallel and in the perpendicular case. They are linear functions of the parameter Wi, which means, that they vanish in the limit of zero shear rate. This is different in the orthogonal configuration. For $\phi = \pi/4$ and $\mathbf{R}_{\pi/4} = \mathbf{Q}$ the correlation functions are given by the expressions:

$$\langle \tilde{x}_1(0)\tilde{y}_1(t)\rangle = \frac{g_{1,1}e^{-\lambda_1 t}}{8\sqrt{\mu^2 - 2\mu\mathrm{Wi}}} - \frac{g_{2,1}e^{-\lambda_2 t}}{8\sqrt{\mu^2 - 2\mu\mathrm{Wi}}}$$
$$+ \frac{g_{4,1}e^{-\lambda_4 t}}{8\sqrt{\mu^2 + 2\mu\mathrm{Wi}}} - \frac{g_{5,1}e^{-\lambda_5 t}}{8\sqrt{\mu^2 + 2\mu\mathrm{Wi}}}, \tag{42a}$$

$$\langle \tilde{y}_1(0)\tilde{x}_1(t)\rangle = \frac{g_{1,2}e^{-\lambda_1 t}}{8\sqrt{\mu^2 - 2\mu\mathrm{Wi}}} - \frac{g_{2,2}e^{-\lambda_2 t}}{8\sqrt{\mu^2 - 2\mu\mathrm{Wi}}}$$
$$+ \frac{g_{4,2}e^{-\lambda_4 t}}{8\sqrt{\mu^2 + 2\mu\mathrm{Wi}}} - \frac{g_{5,2}e^{-\lambda_5 t}}{8\sqrt{\mu^2 + 2\mu\mathrm{Wi}}}. \tag{42b}$$

In the limit of very large particle distances, when $\mu \to 0$, $\langle \tilde{x}_1(0)\tilde{y}_1(t)\rangle$ and $\langle \tilde{y}_1(0)\tilde{x}_1(t)\rangle$ resemble the one-particle case given by eq. (31), whereas in the limit Wi $\to 0$ the two functions become equal but do not vanish in contrast to the previous subsections. Instead of the approximate expressions (42) we display in fig. 12 the full numerical solution for these correlation functions. If Wi $= 0$, the identity $\langle \tilde{x}_1(0)\tilde{y}_1(t)\rangle = \langle \tilde{y}_1(0)\tilde{x}_1(t)\rangle$ is obtained, cf. dotted line in fig. 12. For larger values of Wi the two functions resemble the curves shown in fig. 4.

According to eq. (22) and eq. (23) the inclination angle θ of the elliptical positional probability distribution is determined by the static single-particle correlation functions, which depend on the trap distance d. In fig.13 $\tan(\theta)$ is shown as a function of the parameter $\mu = 3a/(4d)$ for different trap configurations. The analytical expression from the parallel case (solid line) is
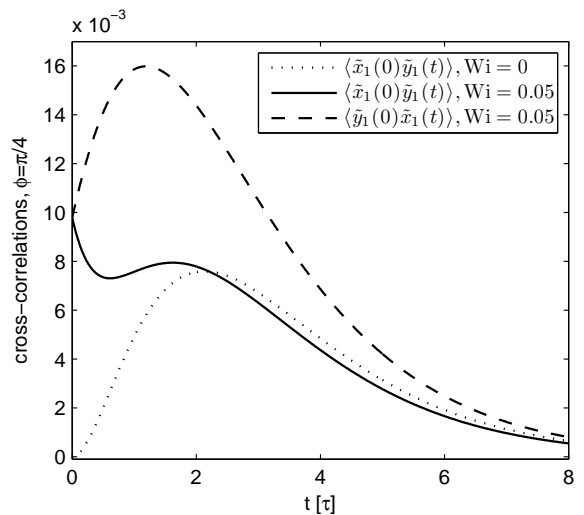

FIG. 12. Single-particle correlations between orthogonal displacements in the shear plane for different Weissenberg numbers, $\phi = \pi/4$ and $d = 4a$. In contrast to the parallel or the perpendicular case, $\langle \tilde{x}_1(0)\tilde{y}_1(t)\rangle$ and $\langle \tilde{y}_1(0)\tilde{x}_1(t)\rangle$ remain finite for Wi $= 0$.
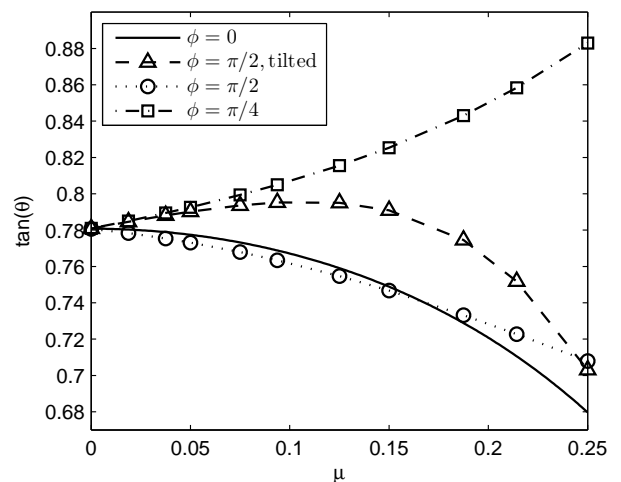

FIG. 13. The inclination angle of the single particle distribution, as given by eq. (22), is shown as a function of the parameter μ. For Wi $= 1/2$ the exact results for the different setups described in the text are compared.

compared with the full numerical solutions for the other setups. For $\phi = \pi/2$ (circles) the monotonous decrease of $\tan(\theta)$ is weaker than for $\phi = 0$. For the tilted configuration given by eq. (38) θ has a broad maximum (triangles), whereas in the oblique case, $\phi = \pi/4$, the inclination angle is increasing continuously with increasing μ (squares).

The inter-particle cross-correlations in parallel directions are again anti-correlated in the present case. For
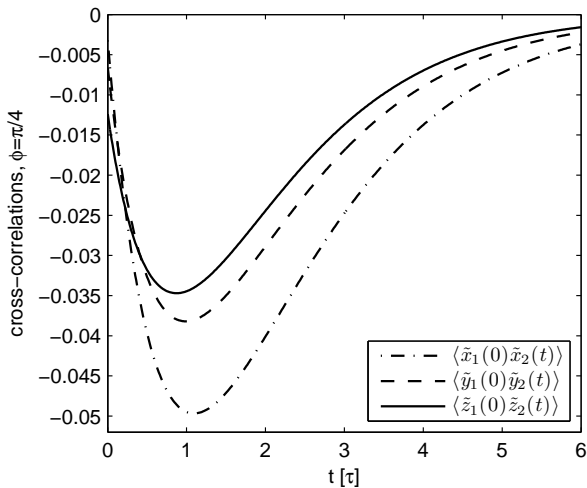
FIG. 14. Inter-particle cross-correlations in the oblique case for $d = 4a$ and Wi $= 1/2$. In the limit Wi $= 0$, $\langle \tilde{x}_1(0)\tilde{x}_2(t) \rangle$ and $\langle \tilde{y}_1(0)\tilde{y}_2(t) \rangle$ become equal.
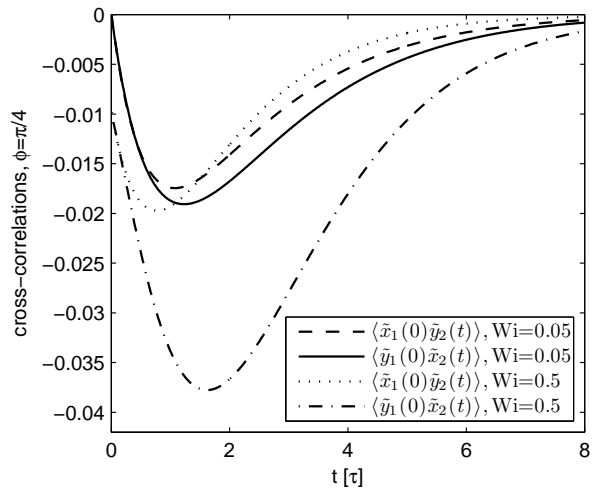

FIG. 15. Cross-correlations in the oblique case for $d = 4a$ and different Weissenberg numbers. The amplitude of $\langle \tilde{y}_1(0)\tilde{x}_2(t) \rangle$ is increasing much stronger with increasing values of Wi than the amplitude of $\langle \tilde{x}_1(0)\tilde{y}_2(t) \rangle$.

the approximation $\mathbf{R}_{\pi/4} = \mathbf{Q}$, we obtain:

$$\langle \tilde{x}_1(0)\tilde{x}_2(t) \rangle = \frac{g_{1,1}e^{-\lambda_1 t}}{8\mu} + \frac{g_{2,1}e^{-\lambda_2 t}}{8\mu}$$
$$- \frac{g_{4,1}e^{-\lambda_4 t}}{8\mu} - \frac{g_{5,1}e^{-\lambda_5 t}}{8\mu}, \quad (43a)$$

$$\langle \tilde{y}_1(0)\tilde{y}_2(t) \rangle = \frac{g_{1,2}e^{-\lambda_1 t}}{8(\mu - 2\text{Wi})} + \frac{g_{2,2}e^{-\lambda_2 t}}{8(\mu - 2\text{Wi})}$$
$$- \frac{g_{4,2}e^{-\lambda_4 t}}{8(\mu + 2\text{Wi})} - \frac{g_{5,2}e^{-\lambda_5 t}}{8(\mu + 2\text{Wi})}, \quad (43b)$$

$$\langle \tilde{z}_1(0)\tilde{z}_2(t) \rangle = \frac{1}{4}\left(e^{-\lambda_3 t} - e^{-\lambda_6 t} \right). \quad (43c)$$

The eqs. (43) indicate that these correlations are different from each other, similar to the perpendicular case. The correlation functions for the correct $\mathbf{R}_{\pi/4}$ are shown in fig. 14.

The cross-correlations $\langle \tilde{x}_1(0)\tilde{y}_2(t) \rangle$ and $\langle \tilde{y}_1(0)\tilde{x}_2(t) \rangle$ show the strongest dependence on the orientation of the trapped particles with respect to the flow direction. If $\phi = \pi/4$, they have one minimum each, which is different from the case $\phi = 0$ and from the tilted configuration (38). Within the approximation, the functions are given

by:

$$\langle \tilde{x}_1(0)\tilde{y}_2(t) \rangle = \frac{g_{1,1}e^{-\lambda_1 t}}{8\sqrt{\mu^2 - 2\mu\text{Wi}}} - \frac{g_{2,1}e^{-\lambda_2 t}}{8\sqrt{\mu^2 - 2\mu\text{Wi}}}$$
$$- \frac{g_{4,1}e^{-\lambda_4 t}}{8\sqrt{\mu^2 + 2\mu\text{Wi}}} + \frac{g_{5,1}e^{-\lambda_5 t}}{8\sqrt{\mu^2 + 2\mu\text{Wi}}}, \quad (44a)$$

$$\langle \tilde{y}_1(0)\tilde{x}_2(t) \rangle = \frac{g_{1,2}e^{-\lambda_1 t}}{8\sqrt{\mu^2 - 2\mu\text{Wi}}} - \frac{g_{2,2}e^{-\lambda_2 t}}{8\sqrt{\mu^2 - 2\mu\text{Wi}}}$$
$$- \frac{g_{4,2}e^{-\lambda_4 t}}{8\sqrt{\mu^2 + 2\mu\text{Wi}}} + \frac{g_{5,2}e^{-\lambda_5 t}}{8\sqrt{\mu^2 + 2\mu\text{Wi}}}. \quad (44b)$$

As illustrated by the numerical results for the correct $\mathbf{R}_{\pi/4}$ in fig. 15, it is remarkable that $\langle \tilde{x}_1(0)\tilde{y}_2(t) \rangle$ does not change very much with the Weissenberg number, while the amplitude of $\langle \tilde{y}_1(0)\tilde{x}_2(t) \rangle$ increases with Wi. Their asymptotic behavior for Wi $\to 0$ is similar to the single-particle correlations given by eqs. (42).

IV. CONCLUSION

In this work we investigated the dynamics of two Brownian particles, each trapped by a harmonic potential and exposed to a linear shear flow. The one-particle and the inter-particle positional correlation functions, which can be measured in an experiment, were calculated by solving an appropriate Langevin model. We discussed the correlations in detail as a function of the distance between the two traps, as a function of the Weissenberg number Wi, and for three different configurations, where the vector connecting the two potential minima was either parallel, perpendicular, or oblique with respect to the flow

direction. This relative orientation strongly affects the time-dependence of the correlation functions. For the parallel configuration exact analytical expressions were presented. Otherwise, we provided numerical solutions and analytical approximations for the correlation functions.

Although the stochastic forces in our model were assumed to be uncorrelated along orthogonal directions, we found a coupling between perpendicular particle displacements caused by the shear flow, similar to that in Ref. [33]. The resulting shear-induced cross-correlations depend linearly on the Weissenberg number, Wi, and occur also between orthogonal fluctuations of different particles. These inter-particle correlations have zero, one, or two extrema as a function of time, depending on the particle configuration. Besides generating new cross-correlations, the shear flow causes a contribution proportional to Wi^2 in the correlation functions of particle fluctuations along parallel directions.

Due to the hydrodynamic interaction between the two particles the magnitudes of the one-particle correlations are enhanced with decreasing trap distance d, while in the limit of large distances the single-particle results presented in Ref. [33] were recovered. Moreover, we found a significant impact of the parameter d on the positional probability distribution of each particle in the shear flow. The shape of the elliptical distribution is tilted and stretched when the two particles approach each other in the parallel configuration. The same effect is observed when the shear rate is increased. So the shear-flow effects are enhanced by the presence of a second particle. In the oblique configuration the opposite effect is observed.

The shear-induced cross-correlations investigated in this work are of the same origin as the correlations between orthogonal fluctuations of a single freely floating particle as discussed in Ref. [30, 32]. However, if the Brownian particles are trapped, a direct experimental detection of these correlations becomes possible. This has been achieved recently in Ref. [34], where two polystyrene latex spheres were trapped by optical tweezers and exposed to a linear shear flow in a special microfluidic device. With this setup the cross-correlations of the positional fluctuations for the parallel case, as shown in fig. 7, were measured directly for the first time. Moreover, we predict an additional extremum for the shear-induced inter-particle correlations, if the two particles are trapped perpendicular to the flow lines, cf. fig. 11.

The two hydrodynamically interacting beads are treated as point-particles. In forthcoming works, the presented results on the shear-induced correlations are extended by taking the finite particle extension into account. Preliminary investigations show that the effects of particle rotations do not change the major trends in this work [55], and for small Wi the rotation can be neglected anyhow.

The present article provides insight on the Brownian motion of two trapped particles that might be useful for the analysis of the stochastic dynamics of a bead-spring model for polymers too, where the Brownian particles are connected along a chain and fluctuate around some mean distance to their next neighbors. The fluctuations along and perpendicular to the connection vector between two neighboring beads may exhibit similar correlations as for the three model configurations investigated in this work, cf. fig. 1. In this spirit, a profound analysis of the stochastic motion of a bead-spring model in a linear shear flow is an interesting task and may contribute further to the understanding of polymer dynamics.

[1] G. Taylor, Proc. R. Soc. London A **219**, 186 (1953).

[2] J. Ottino and S. Wiggins, Phil. Trans. R. Soc. Lond. A **362**, 923 (2004).

[3] A. Groisman and V. Steinberg, Nature **410**, 905 (2001).

[4] J. K. G. Dhont, *An Introduction to Dynamics of Colloids* (Elsevier, Amsterdam, 1996).

[5] M. Doi and S. F. Edwards, *The Theory of Polymer Dynamics* (Clarendon Press, Oxford, 1986).

[6] J. C. Meiners and S. R. Quake, Phys. Rev. Lett. **82**, 2211 (1999).

[7] M. Reichert and H. Stark, Phys. Rev. E **69**, 031407 (2004).

[8] D. Smith, H. Babcock, and S. Chu, Science **283**, 1724 (1999).

[9] P. G. deGennes, Science **276**, 1999 (1997).

[10] A. Groisman and V. Steinberg, Nature **405**, 53 (2000).

[11] T. Perkins, D. Smith, R. Larson, and S. Chu, Science **268**, 83 (1995).

[12] F. Brochard-Wyart, Europhys. Lett. **23**, 105 (1993).

[13] R. G. Larson, T. T. Perkins, D. E. Smith, and S. Chu, Phys. Rev. E **55**, 1794 (1997).

[14] R. Rzehak, D. Kienle, T. Kawakatsu, and W. Zimmermann, Europhys. Lett. **46**, 821 (1999).

[15] R. Rzehak, W. Kromen, T. Kawakatsu, and W. Zimmermann, Eur. Phys. J. E **2**, 3 (2000).

[16] D. Kienle and W. Zimmermann, Macromolecules **34**, 9173 (2001).

[17] R. Rzehak and W. Zimmermann, Phys. Rev. E **68**, 021804 (2003).

[18] P. Szymczak and M. Cieplak, J. Chem. Phys. **125**, 164903 (2006).

[19] D. Kienle, R. Rzehak, and W. Zimmermann, subm. to New. J. Phys. , (2010).

[20] P. Doyle, B. Ladoux, and J. Viovy, Phys. Rev. Lett. **84**, 4769 (2000).

[21] M. Webster and J. Yeomans, J. Chem. Phys. **122**, 164903

(2005).

[22] R. Delgado-Buscalioni, Phys. Rev. Lett. **96**, 088303 (2006).

[23] C. A. Lueth and E. S. G. Shaqfeh, Macromolecules **42**, 9170 (2009).

[24] Y. Zhang *et al.*, J. Chem. Phys. **130**, 234902 (2009).

[25] J. Hur, E. Shaqfeh, and R. Larson, J. Rheol. **44**, 713 (2000).

[26] C. Schroeder, R. Teixeira, E. Shaqfeh, and S. Chu, Phys. Rev. Lett. **95**, 018301 (2005).

[27] S. Gerashchenko and V. Steinberg, Phys. Rev. Lett. **96**, 038304 (2006).

[28] B. Eckhardt and R. Pandit, Eur. Phys. J. B **33**, 373 (2003).

[29] G. Khujadze, M. Oberlack, and G. Chagelishvili, Phys. Rev. Lett. **97**, 034501 (2006).

[30] K. Miyazaki and D. Bedeaux, Physica **217A**, 53 (1995).

[31] G. Subramanian and J. Brady, Physica **334A**, 343 (2004).

[32] Y. Drossinos and M. W. Reeks, Phys. Rev. E **71**, 031113 (2005).

[33] L. Holzer, J. Bammert, R. Rzehak, and W. Zimmermann, Phys. Rev. E **81**, 041124 (2010).

[34] A. Ziehl *et al.*, Phys. Rev. Lett. **103**, 230602 (2009).

[35] R. Simmons, J. Finer, S. Chu, and J. Spudich, Biophys. J. **70**, 1813 (1996).

[36] S. Henderson, S. Mitchell, and P. Bartlett, Phys. Rev. Lett. **88**, 088302 (2002).

[37] E. R. Dufresne, T. M. Squires, M. Brenner, and D. G. Grier, Phys. Rev. Lett. **85**, 3317 (2000).

[38] T. Franosch and S. Jeney, Phys. Rev. E **79**, 031402

[39] J. Crocker *et al.*, Phys. Rev. Lett. **85**, 888 (2000).

[40] P. T. Korda, M. B. Taylor, and D. G. Grier, Phys. Rev. Lett. **89**, 128301 (2002).

[41] M. P. MacDonald, G. C. Spalding, and K. Dholakia, Nature **426**, 421 (2003).

[42] J. Bammert, S. Schreiber, and W. Zimmermann, Phys. Rev. E **77**, 042102 (2008).

[43] J. Bammert and W. Zimmermann, Eur. Phys. J. E **28**, 331 (2009).

[44] J. Crocker and D. Grier, J. Colloid Interf. Sci. **179**, 298 (1996).

[45] B. Lukic *et al.*, Phys. Rev. Lett. **95**, 160601 (2005).

[46] M. Atakhorrami, G. H. Koenderink, C. F. Schmidt, and F. C. MacKintosh, Phys. Rev. Lett. **95**, 208302 (2005).

[47] S. Chu, Science **253**, 861 (1991).

[48] M. Polin, Y. Roichman, and D. G. Grier, Phys. Rev. E **77**, 051401 (2008).

[49] G. G. Stokes, Trans. Cambridge Phil. Soc. **IX**, 8 (1850).

[50] L. D. Landau and E. M. Lifschitz, *Lehrbuch der Theoretischen Physik: Hydrodynamik*, 2nd ed. (Akademie Verlag, Berlin, 1987).

[51] L. Holzer, Ph.D. thesis, Universität Bayreuth, 2009.

[52] R. Rzehak and W. Zimmermam, Physica **324A**, 495 (2003).

[53] S. Martin, M. Reichert, H. Stark, and T. Gisler, Phys. Rev. Lett. **97**, 248301 (2006).

[54] A. Ziehl, Ph.D. thesis, Universität des Saarlandes, 2010.

[55] S. Schreiber, J. Bammert, P. Peyla, and W. Zimmermann, in preparation (2010).